Development of Nd^{3+}-doped Monoclinic Dimolybdates $La_2Mo_2O_9$ as Optical Materials

Małgorzata Guzik[a], Magdalena Bieza[a], Elżbieta Tomaszewicz[b], Yannick Guyot[c], and Georges Boulon[c]

[a] Faculty of Chemistry, University of Wrocław, 14 F. Joliot-Curie Street, 50-383 Wrocław, Poland

[b] Department of Inorganic and Analytical Chemistry, West Pomeranian University of Technology, Al. Piastów 42, 71-065 Szczecin, Poland

[c] Institute Light Matter, UMR5306 CNRS-University Lyon1, University of Lyon, 69622 Villeurbanne, France

Reprint requests to Dr. Małgorzata Guzik. Fax: +48 71 328 23 48. E-mail: goguzik@poczta.fm

Z. Naturforsch. **2014**, *69b*, 193 – 204 / DOI: 10.5560/ZNB.2014-3290
Received October 9, 2013

The work presented is mainly focused on synthesis and study of structural and optical properties of microcrystalline Nd^{3+}-doped monoclinic dilanthanum dimolybdate at both room and cyrogenic temperatures (4 K and 77 K). These compounds might be useful for application in the future as optical materials and also as transparent ceramics when the structure is cubic. The Nd^{3+}-doped phases with monoclinic structure (α-form, space group $P2_1$, unit cell parameters $a = 7.1426$, $b = 7.1544$, $c = 7.1618$ Å and $\beta = 89.538°$) were observed for a concentration of the optically active ions equal to 5 %. When the concentration of the Nd^{3+} ions is higher than 15 %, a cubic structure is formed (β-form, space group $P2_13$, with the lattice parameter $a = 7.155 \pm 0.005$ Å). A series of Nd^{3+}-doped $La_2Mo_2O_9$ phases with different concentration of Nd^{3+} were prepared using conventional solid-state reactions. The formation of phase-pure Nd^{3+}-doped $La_2Mo_2O_9$ has been monitored by powder X-ray diffraction, DSC, SEM, Raman, and FT-IR absorption techniques. High-resolution absorption and emission spectra, as well as the dynamics of the Nd^{3+} excited states characterized by decay time measurements were recorded from room temperature to 4 K. At least two slightly different crystallographic sites are available for the Nd^{3+} ions. First results show that this new Nd^{3+}-doped monoclinic $La_2Mo_2O_9$ molybdate phosphor is promising for applications of ultra-short pulse lasers.

Key words: Nd^{3+} Emission, Monoclinic System, Molybdates, Near-infrared Luminescence, Powder Lasers

Introduction

Research on advanced optical materials is increasing. As an example, the progress in solid-state laser sources like laser-diode (LD)-pumped solid-state lasers (DPSSL) including the development of new materials and high-power laser diodes has led to high-power and tunable systems. Different types of laser devices are widely used in industrial, medical, military and scientific fields. Even though more than 50 years have passed since the invention of the first ruby laser, this research topic is still timely. It is well known that tungstates and molybdates are excellent host structures to be doped by rare-earth ions. The first continuously operating crystal laser doped with Nd^{3+} ion was reported in 1961 and based exactly on $CaWO_4$ tungstate. Alkali and trivalent lanthanide metal double tungstates $MRE(WO_4)_2$ (M = alkali metal, RE = Y, Gd, Lu) can be highly doped with optically active rare-earth ions such as Nd^{3+}, Dy^{3+}, Ho^{3+}, Er^{3+}, Tm^{3+} or Yb^{3+} to form materials for laser purposes [1 – 3]. Both neodymium- and ytterbium-doped $KGd(WO_4)_2$ (KGW) and $KY(WO_4)_2$ (KYW) single crystals became very important laser materials for the near-infrared region. Their emission cross-sections are higher than that of YAG at 1.067 μm. Such laser sources emitting at 1.351 μm can be used for medical applications. Thus, especially KGW and KYW tungstates doped with Yb^{3+} ions show high potential for light generation or amplification [4 – 6].

Cubic garnet crystals, especially Nd^{3+}:$Y_3Al_5O_{12}$ (YAG) laser crystals, are commercially produced by the Czochralski method. In this case, the Nd^{3+} concentration that affects laser performances, is strongly limited to values between 0.2 – 1.4 at.-% of Nd^{3+} as a result of the segregation coefficient [7]. Consequently, the technique of sintering mono-crystalline grains to large optically transparent ceramics was developed. Polycrystalline ceramics possess advantages regarding their size, mechanical strength and manufacturing costs. Ikesue *et al.* [8, 9] first demonstrated the possibility of fabricating transparent Nd^{3+}:YAG ceramics with sufficient quality for solid-state lasers showing reasonable efficiency. More recently, a number of studies have shown that transparent polycrystalline Nd^{3+}:YAG ceramics are equivalent to single crystals grown by the Czochralski method [10 – 12].

To the best of our knowledge, no transparent ceramics of rare-earth-doped tungstates and molybdates are known in the literature. Thus, the fabrication of such ceramics poses a great challenge. To obtain transparent ceramics, two conditions must be satisfied: the compounds have to crystallize in the cubic system, and the size of the crystallites must be in the order of tens of nanometers.

The family of rare-earth-doped molybdates, $RE_2Mo_2O_9$, where RE = La, Ce, Pr, Nd, and Gd, known in the literature was only examined as oxide ion conductors. Thermal, structural and transport properties of the fast oxide ion conductors, $La_{2-x}RE_xMo_2O_9$ (RE = Y, Nd, and Gd), were reported by Georges *et al.* [13]. The authors have reported the existence of the LAMOX family, a new series of oxide ion conductors obtained by various cationic substitutions on $La_2Mo_2O_9$. This compound was first reported by Fournier *et al.* [14] who prepared it in 1970 using conventional ceramic synthesis. The authors reported also that the diffraction pattern of this compound can be indexed in the cubic system with the lattice parameter $a = 7.155 \pm 0.005$ Å. More recently, Lacorre *et al.* have shown that it is possible to prepare $La_2Mo_2O_9$ by direct ball milling synthesis [15]. Then, Kuang *et al.* [16] reported the preparation of nanoscaled $La_2Mo_2O_9$ powder and studied its catalytic activity. The crystal structures of $La_2Mo_2O_9$ polymorphs were determined by Goutenoire *et al.* using X-ray, neutron, and electron diffraction [17]. This compound presents a reversible phase transformation at 580 °C from a low-temperature monoclinic form α-$La_2Mo_2O_9$ to a high-temperature modification β-$La_2Mo_2O_9$, which has a cubic structure (at 617 °C, space group $P2_13$ with $a = 7.2014(5)$ Å and $Z = 2$) derived from the β-$SnWO_4$ structure. A few years later Corbel *et al.* presented a comprehensive survey of Nd^{3+} substitution in $La_2Mo_2O_9$ oxide ion conductors, where they provided evidence for a metastability phenomenon in an extended compositional range of the Nd^{3+}-doped $La_2Mo_2O_9$ solid solution [18]. Also the effect of partial substitution, up to 20 %, of La^{3+} by Eu^{3+} on the phase stability, thermal expansion and transport properties of $La_2Mo_2O_9$ were investigated [19], but no investigations of the optical properties have been reported until now.

Being a first part of a general study this paper deals with fabrication and investigation, for the first time, of the optical properties of Nd^{3+}-doped $La_2Mo_2O_9$ prepared by conventional solid-state reaction. We present the data of the low-temperature monoclinic α-form while those of the high-temperature cubic β-form will follow in a subsequent paper.

Experimental Part

Synthesis of microcrystalline $La_{2-x}Nd_xMo_2O_9$ solid solutions

For the synthesis of microcrystalline powder materials the following commercial metal oxides were used: lanthanum oxide (La_2O_3, 99.999 %, Alfa Aesar), neodymium oxide (Nd_2O_3, 99.99 %, Alfa Aesar) and molybdenum oxide (MoO_3, 99.95 %, Alfa Aesar). Before starting the synthesis, lanthanum oxide and neodymium oxide were calcined at 850 °C, in two 12-hour cycles to remove adsorbed moisture and carbon dioxide. Weighed in appropriate molar ratios, the oxides were homogenized by grinding in an agate mortar. Next, the obtained mixtures were heated in ceramic crucibles in air in the following cycles: 550 °C (12 h), 600 °C (12 h), 650 °C (12 h), 700 °C (12 h) and 750 °C (12 h), 800 °C (12 h), 900 °C (12 h), and 1000 °C (3 × 12 h). After each heating cycle, the samples were cooled to room temperature, weighed, and then ground in an agate mortar. Several regrinding and heating sequences at the temperatures mentioned above were necessary in order to obtain high-purity phases. The synthesis of the solutions was started at a relatively low temperature (550 °C) considering the low melting point of pure MoO_3 (*ca.* 760 °C) and the possible weight loss caused by evaporation of this oxide (MoO_3 shows a high vapor pressure at temperatures slightly below the melting point). The phase composition of the samples under study was controlled after heating them at temperatures of 800, 900 and 1000 °C by using powder X-ray diffraction (PXRD). The

Model of $La_{2-x}Nd_xMo_2O_9$ solid solution; value of x parameter	Initial content of $Nd_2O_3/La_2O_3/MoO_3$ mixtures (mol-%)			Concentration of Nd^{3+} ions in $La_2Mo_2O_9$:Nd^{3+} (mol-%)
	Nd_2O_3	La_2O_3	MoO_3	
$La_{1.80}Nd_{0.20}Mo_2O_9$; $x = 0.20$	3.33	30.00	66.67	10
$La_{1.86}Nd_{0.14}Mo_2O_9$; $x = 0.14$	2.33	31.00	66.67	7
$La_{1.90}Nd_{0.10}Mo_2O_9$; $x = 0.10$	1.66	31.67	66.67	5
$La_{1.94}Nd_{0.06}Mo_2O_9$; $x = 0.06$	1.00	32.33	66.67	3
$La_{1.96}Nd_{0.04}Mo_2O_9$; $x = 0.04$	0.66	32.67	66.67	2
$La_{1.97}Nd_{0.03}Mo_2O_9$; $x = 0.03$	0.50	32.83	66.67	1.5
$La_{1.98}Nd_{0.02}Mo_2O_9$; $x = 0.02$	0.33	33.00	66.67	1.0
$La_{1.99}Nd_{0.01}Mo_2O_9$; $x = 0.01$	0.16	33.17	66.67	0.5
$La_{1.996}Nd_{0.004}Mo_2O_9$; $x = 0.004$	0.06	33.27	66.67	0.2

Table 1. Content of $Nd_2O_3/La_2O_3/MoO_3$ initial mixtures, formulae of the $La_{2-x}Nd_xMo_2O_9$ solid solutions and the concentration of Nd^{3+} in $La_2Mo_2O_9$ matrix.

preparation of the $La_{2-x}Nd_xMo_2O_9$ solid solutions (later labeled as Nd^{3+}-doped $La_2Mo_2O_9$ or Nd^{3+}:$La_2Mo_2O_9$) can be described by the following equation:

$$(1-x/2)\,La_2O_{3(s)} + x/2\,Nd_2O_{3(s)} + 2\,MoO_{3(s)} \rightarrow La_{2-x}Nd_xMo_2O_{9(s)} \quad (1)$$

Table 1 presents the content of the initial mixtures of $Nd_2O_3/La_2O_3/MoO_3$, the formula of the investigated solid solutions and the concentrations of Nd^{3+} ions (in mol-%) in $La_{2-x}Nd_xMo_2O_9$.

Characterization

To identify the obtained phases, PXRD patterns were collected at room temperature by using a D8 Advance X-ray diffractometer (Bruker). The measurements were performed in the 2θ range $10-70^\circ$ with a scan width of 0.008° per step and a counting time of 5 s per step. For the experiments nickel-filtered CuK_α radiation ($K_{\alpha 1+2}$, $\lambda = 0.15418$ nm) was used. Powder diffraction patterns of some Nd^{3+}-doped $La_2Mo_2O_9$ solid solutions with different contents of the optically active ion (Nd^{3+}) were compared with the simulated XRD pattern of monoclinic α-$La_2Mo_2O_9$ from the inorganic crystal structure database (ICSD).

Simultaneous DTA and TG measurements were carried out on a TA Instruments thermal analyzer (model SDT 2960) at a heating and cooling rate of 10 °C min^{-1} in air (maximum temperature 1000 °C, air flow rate 110 mL h^{-1}) using alumina crucibles. DSC studies were performed on a TA Instruments microcalorimeter (model DSC 2010) at a heating and cooling rate of 10 °C min^{-1} (maximum temperature 600 °C) in closed aluminum capsules (argon flow rate 110 mL h^{-1}, purity 99.999 %).

Scanning electron microscopy studies were carried out on a Hitachi S-3400N instrument equipped with an energy dispersive X-ray spectroscopy (EDX) EDAX analyzer. The powders were coated with a thin gold alloy layer to facilitate conductivity.

FT-IR spectra of powdered samples in the $1000-80$ cm^{-1} spectral range were measured using a Specord-M-80 spectrometer (Carl Zeiss Jena). The powdered samples were mixed with Nujol oil (a mixture of liquid hydrocarbons) and then pressed into pellets. A Nicolet Magna 860 FT-IR/FT Raman spectrometer was used for the measurements recorded at an excitation line of 1.064 microns with a capacity of about 400 – 500 mW. The apparatus was equipped with a CaF_2 beam splitter and an InGaSe detector. The polycrystalline samples were placed in a quartz tube. The spectral resolution of the Raman and IR measurements was 2 cm^{-1}.

Absorption spectra in the 200 – 2500 nm spectral range were recorded at 4 and 293 K on a Cary-Varian 5000 Scan spectrometer equipped with an Oxford CF 1204 helium flow cryostat. The pellets used for the absorption measurements were prepared under 20 MPa pressure.

Emission measurements under pulsed laser excitation (OPO laser, EKSPLA NT342, 10Hz, 7 ns) were performed with the help of a cooled germanium cell (Northcoast) coupled to a boxcar SRS250. For the comparative measurements of the integral intensity a CW titanium sapphire laser coupled with an IR Hamamatsu CCD camera with a ruled grating of 900 lines per mm line density at the 1300 nm blaze wavelength was used. The emission spectra were recorded both at room as well as at liquid nitrogen temperature.

The luminescence decay curves were recorded under pulsed laser excitation (OPO laser, EKSPLA NT342, 10 Hz, 7 ns). Detecting the fluorescence intensity around 1.06 μm was possible with the help of a fast cooled germanium cell (Northcoast) coupled to a Lecroy 342 digital oscilloscope. The luminescence decay curves were recorded at room and liquid nitrogen temperature.

Results and Discussion

Structural analysis of Nd^{3+}-doped $La_2Mo_2O_9$ molybdate

Morphology of the powder samples

As a result of the solid-state reaction, micropowders with different contents of neodymium and lanthanum

were produced. The morphology of the Nd^{3+}-doped $La_2Mo_2O_9$ microcrystallites was investigated by scanning electron microscopy (SEM). Fig. 1 presents SEM micrographs of 3 % Nd^{3+}-doped $La_2Mo_2O_9$. The micropowders consisted of agglomerated irregular particles, although a type of boundary between the microcrystals can be seen. The overview picture shows separated particles and loose clusters. The average size of the particles is around a few micrometers ($\sim 3-8\,\mu$m). Increased concentrations of the dopant caused an increase of the size of the grains by aggregation of the smaller grains into asymmetrical forms. A similar tendency was observed by us for the Nd^{3+}-doped tungstates also obtained by solid-state reaction as reported recently [20, 21].

XRD analysis

The La_2O_3-MoO_3 systems were first reported by Fournier *et al.* in 1970, who prepared them using conventional ceramic synthesis. They first presented a phase diagram of the La_2O_3-MoO_3 system [14]. In order to obtain $La_2Mo_2O_9$, the molar ratio of La_2O_3/MoO_3 has to be 1 : 2. The structure of room-temperature α-$La_2Mo_2O_9$ was solved for the first time by Evans *et al.* [22]. The single-crystal X-ray diffraction studies of α-$La_2Mo_2O_9$ have shown that at room temperature all reflections could be indexed using a monoclinic cell, space group $P2_1$, with the unit cell parameters $a = 14.325(3)$, $b = 21.482(4)$, $c = 28.585(6)$ Å, and $\beta = 90.40(3)^\circ$. This $2 \times 3 \times 4$ superstructure relative to the cubic high-temperature β-form and a small monoclinic distortion have also been suggested by electron diffraction and neutron diffraction studies published previously [17]. Several substitutions possible on both cationic [23] and anionic [24] sites of $La_2Mo_2O_9$ stabilize the high-temperature β-form. Georges *et al*. reported that for Nd^{3+} substitution the monoclinic α-form is retained at room temperature over the whole compositional range. Upon Gd and Yb substitutions above a certain doping level, the suppression of the phase transition and stabilization of the cubic β-$La_2Mo_2O_9$ at room temperature are achieved. However, these results are in contradiction with that reported by Corbel because the Nd^{3+} doping level in this host structure is also limited. The observation of Corbel differs from that of Georges *et al*. because in the whole compositional range explored ($0 < x \leq 1$), the stabilization of the cubic β-form was never observed

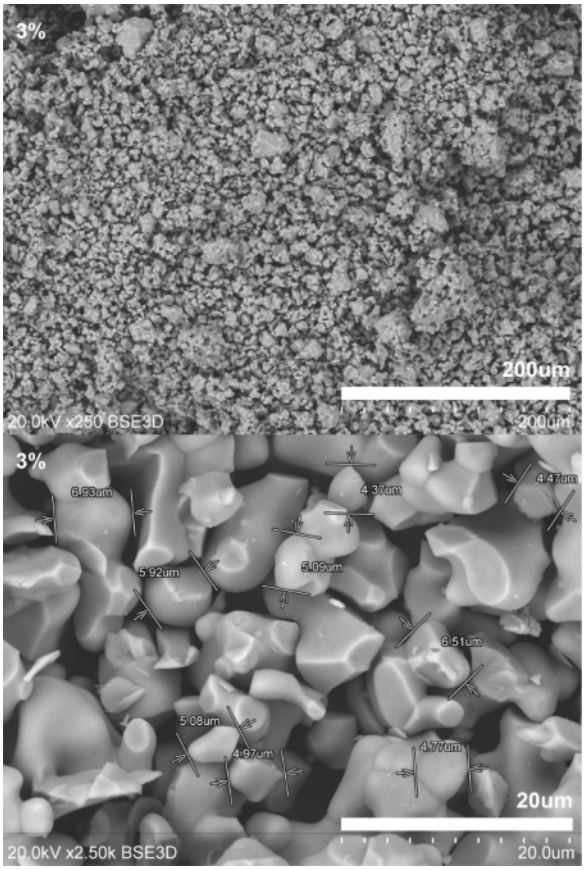

Fig. 1. Scanning electron micrograph and particle sizes of the 3 mol-% Nd^{3+}-doped $La_2Mo_2O_9$ solid solution.

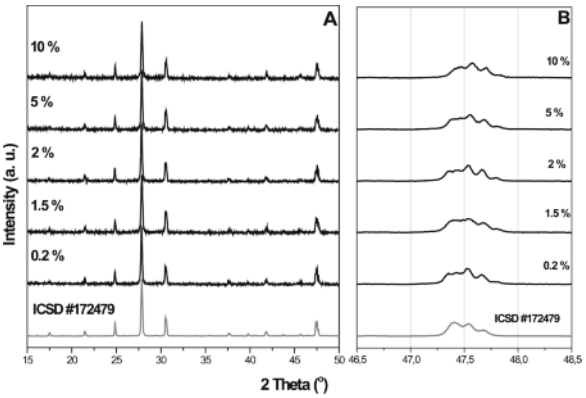

Fig. 2. Room-temperature powder X-ray diffraction patterns (CuK_α; $\lambda = 0.15418$ nm) of some Nd^{3+}-$La_2Mo_2O_9$ solid solutions with different contents of the optically active ion (Nd^{3+}) and a simulated XRD pattern of monoclinic α-$La_2Mo_2O_9$ (ICSD 172479) [22] (A) and the pseudo-cubic 231 peak (B).

at room temperature [18]. It appeared when the compositional range range was above $x = 0.35$.

The results obtained by us are in agreement with those of Corbel. We present the room temperature X-ray powder diffraction patterns of Nd^{3+}-doped $La_2Mo_2O_9$ solid solutions in the compositional range ($0.004 \leq x \leq 0.2$). For all mentioned samples, the powder diffraction patterns agree with the diffraction lines of the α-$La_2Mo_2O_9$ low-temperature form. Fig. 2 presents the room temperature X-ray powder diffraction patterns of some $La_2Mo_2O_9$ solid solutions with different Nd^{3+} contents and a simulated XRD pattern for monoclinic α-$La_2Mo_2O_9$ (ICSD 17247) [22] and the pseudo-cubic 231 peak.

DTA-TG and DSC studies

DTA-TG and DSC studies were performed for pure $La_2Mo_2O_9$ and its Nd^{3+}-doped solid solutions. Only one mildly intense endothermic effect was recorded on each DTA curve (not presented here) recorded during controlled heating up to a temperature of 1000 °C for all samples under study. This effect with the onset at 560 °C ($La_2Mo_2O_9$), and at 563 °C (5 % Nd^{3+}-doped $La_2Mo_2O_9$), is connected with a transformation of the monoclinic α- to the cubic β-modification of $La_2Mo_2O_9$. The beginning of a reverse transformation of the β-form to the α-modification (an exothermic effect) observed during controlled cooling of the samples is slightly shifted towards lower temperatures and starts at 546 °C ($La_2Mo_2O_9$), and at 533 °C (5 % Nd^{3+}-doped $La_2Mo_2O_9$). The residues in the crucibles after the DTA-TG examinations were powdery. Fig. 3 shows DSC curves of $La_2Mo_2O_9$ (A_1 – controlled heating; A_2 – controlled cooling) as well as of the Nd^{3+}-doped $La_2Mo_2O_9$ solid solutions with the following Nd^{3+} concentrations: 0.2, 1, 3, 5, and 10 %. Both DTA and DSC studies have shown that the polymorphic change of α-$La_2Mo_2O_9$ to the β-form takes place at 560 °C. This temperature is slightly lower than the previously published one [17]. DSC studies have also clearly demonstrated that the phase transformation is reversible. This fact is confirmed by the appearance of the highly intense exothermic effect at 555 °C on the cooling curve (Fig. 3, curve A_2). On each DSC curve of Nd^{3+}-doped $La_2Mo_2O_9$ solid solutions one such sharp and highly intense endothermic effect was observed. The onset of the endothermic effect varies between 560 and 566 °C, and slightly increases with the Nd^{3+} concentration.

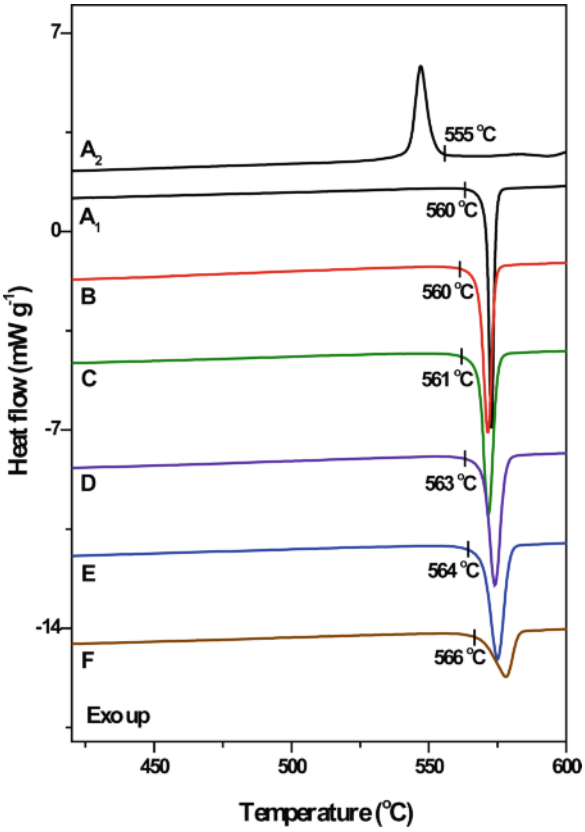

Fig. 3 (color online). DSC curves of pure $La_2Mo_2O_9$ (A1 – controlled heating; A2 – controlled cooling) and Nd^{3+}-doped $La_2Mo_2O_9$ solid solutions for the following Nd^{3+} concentrations (in mol-%): B 0.2; C 1.0; D 3.0; E 5.0; F 10.0.

IR and Raman spectra

Fig. 4 shows the IR and Raman spectra of 0.2 % Nd^{3+}-doped $La_2Mo_2O_9$. In the light of literature information [25] concerning binary and ternary lanthanide molybdates with various types of isolated and joined molybdate polyhedra, the bands with their maxima in the range of 750 – 960 cm^{-1} (Fig. 4) could be assigned to the stretching modes of Mo–O bonds in MoO_4 tetrahedra as well as to the stretching modes of Mo–O bonds in joined MoO_6 octahedra as, *e. g.*, in $[(Mo_2O_9)^{6-}]_\infty$ infinite chains as in $Pr_2Mo_2O_9$ [25]. At the present stage of our studies no structural details can be proposed.

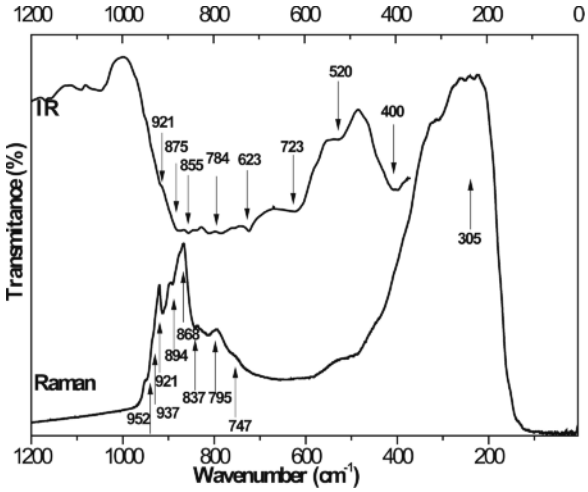

Fig. 4. FT-IR and Raman spectra of 0.2 mol-% Nd^{3+}-doped $La_2Mo_2O_9$ recorded at room temperature.

For the interpretation of the Raman results obtained for Nd^{3+}-doped $La_2Mo_2O_9$, the previous studies made by Mhadhbi were very useful [26]. An analysis of the Raman spectra for the monoclinic α-$La_2Mo_2O_9$ and the cubic β-$La_2Mo_2O_9$ phases as a function of the excitation power and temperature changes has been presented. For monoclinic α-$La_2Mo_2O_9$ recorded at room temperature one can observe three bands with maxima at around 80, 350 and 870 cm^{-1}. With heating of the sample the shape of the spectra changes and stays stable to above 580 °C, where the phase transition (monoclinic to cubic) takes place. The stabilization of the β-$La_2Mo_2O_9$ modification was observed also at room temperature by a different ion substitution. The mentioned phase is well characterized by a significant change of the profile of a band at around 840 cm^{-1} which for the β-$La_2Mo_2O_9$ phase consists of only two peaks, while for the α-$La_2Mo_2O_9$ phase at least four components can be distinguished. Based on this analysis one can conclude that the samples under study correspond to the low-temperature polymorph of $La_2Mo_2O_9$. This fact is in accordance with the results obtained by PXRD diffraction. FT-Raman spectra of Nd^{3+}-doped $La_2Mo_2O_9$ recorded at room temperature are presented in Fig. 4. Broad bands with maxima in the ranges of 160 – 450 and 760 – 960 cm^{-1} are observed. The very strong Raman band in the range of 160 – 450 cm^{-1} is due to the strong luminescence of the Nd^{3+}-doped sample. Because it covers this spectral range, the region where two Raman bands from the $La_2Mo_2O_9$ (80, 350 cm^{-1}) should be observed for the sample under studies, it is not possible to locate these bands. However, the well-developed components corresponding to the vibrations of the MoO_4 units can be observed in the region of 760 – 960 cm^{-1}. According to literature data, the symmetric and asymmetric stretching vibrations of tetrahedral MoO_4 units generate Raman bands at 895 – 950 and 810 – 880 cm^{-1} [27 – 29]. The peak at 930 cm^{-1} suggests the existence of isolated, but distorted MoO_4 tetrahedra. For all compositions we can clearly see six components; however for the lowest concentration of active ion (0.2 %) the components are well resolved.

Optical properties. Evidence of Nd^{3+} multisites

Optical absorption spectra of Nd^{3+} ions in $La_2Mo_2O_9$

Similar to the Eu^{3+} probe ion, the neodymium ion can be used to obtain information about the environment of the metal center in the host structure. On the basis of the number of components for some transitons, *i. e.* the singlet of $^2P_{1/2}$ and the doublet of $^4F_{3/2}$ observed in the low-temperature (4 K) absorption spectra, one can draw conclusions regarding the number of non-equivalent positions occupied by the neodymium ion in the host structure. Fig. 5 presents the energy level scheme of the Nd^{3+} ion with marked $^2P_{1/2}$ and $^4F_{3/2}$ levels which can give rise to transitions useful in structural studies. According to the Judd-Jorgensen statement, the $f-f$ transitions which obey the $\Delta J \leq 2$, $\Delta L = 2$, $\Delta S = 0$ selection rules are most sensitive to the lanthanide ion environment, and are commonly referred to as hypersensitive. Therefore, the intensity of the $^4I_{9/2} \rightarrow {}^4G_{5/2}$ absorption transition of Nd^{3+} is often used as a probe of structural changes, similar to the $^4I_{9/2} \rightarrow {}^4F_{5/2}$ transition in the IR region, which also partially satisfies the selection rule for a hypersensitive transition. In practice the energy of the $^2G_{7/2}$ term is very close to that of the $^4G_{5/2}$ term, thus at room temperature the $^4I_{9/2} \rightarrow {}^4G_{5/2}$ and $^2G_{7/2}$ transitions must be analyzed together. The highest intensity is observed for the hypersensitive $^4I_{9/2} \rightarrow {}^4G_{5/2}$, $^2G_{7/2}$ transitions, due to the structural distortion of the site occupied by Nd^{3+}. The absorption spectra in the 780 – 830 nm range reveal suitable absorption channels for laser diode pumping due to the large broadening of the bands.

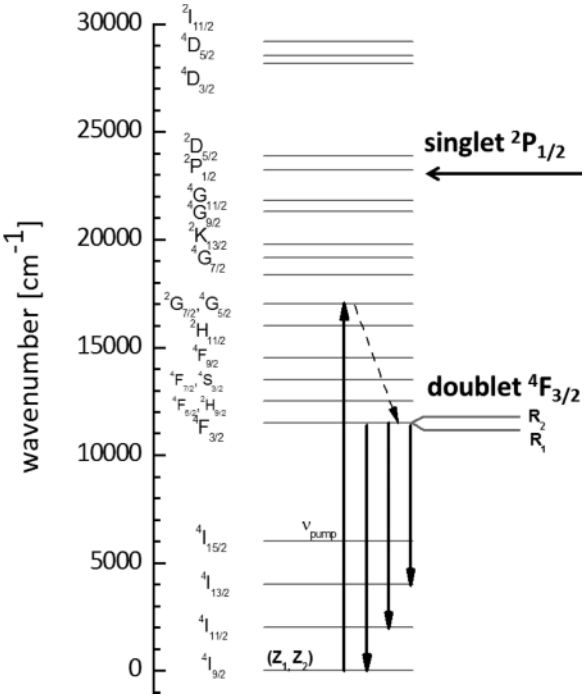

Fig. 5. Energy level scheme of the Nd^{3+} ion with marked special levels ($^2P_{1/2}$ and $^4F_{3/2}$) which may be useful in structural studies.

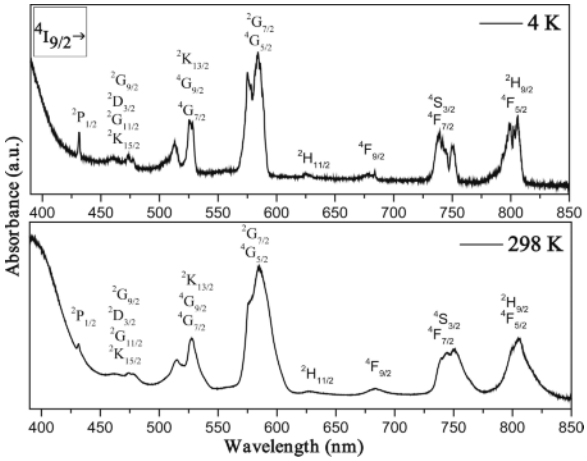

Fig. 6. Absorption spectra of 10 mol-% Nd^{3+}-doped $La_2Mo_2O_9$ recorded at room temperature and 4 K.

Based on the intensity ratio of the $^4I_{9/2} \rightarrow {}^4G_{5/2}$, $^2G_{7/2}$, $^4I_{9/2} \rightarrow {}^4F_{7/2}$, $^4S_{3/2}$ and $^4I_{9/2} \rightarrow {}^4F_{5/2}$, $^2H_{9/2}$ transitions in the IR region, one can draw conclusions regarding the symmetry of the compounds. For highly symmetrical systems, such as O_h and D_{4h}, the intensities of these two transitions in the IR region are about half of those of the $^4I_{9/2} \rightarrow {}^4G_{5/2}$, $^2G_{9/2}$ transitions, while in environments of low symmetry the ratio is significantly higher [30, 31].

From the series of Nd^{3+}-doped $La_2Mo_2O_9$ solid solutions, absorption measurements at 4 K were performed for two concentrations (3 and 10 %). As an example, Fig. 6 shows absorption spectra in the visible and near infrared region at room and low temperature (4 K) recorded for a 10 % Nd^{3+}-doped sample. They correspond to the Nd^{3+} ion transitions from the $^4I_{9/2}$ ground state to the excited states which have been already described in detail in the literature. The most intense band in the spectra with a maximum at 584 nm corresponds to the $^4I_{9/2} \rightarrow {}^4G_{5/2}$, $^2G_{7/2}$ transitions. The intensity ratio between two bands in the IR spectral ranges 710 – 778 nm and 778 – 838 nm and the one in the range 550 – 617 nm is equal to 1 : 2 and indicates high symmetry of the system under investigation. The ratio remains very similar both at room and low temperatures.

The bands in the room-temperature absorption spectra are relatively broad which suggests disordering of the active ions in the structure. At liquid helium temperature the absorption bands are better resolved. Due to the depopulation of the crystal field components of the $^4I_{9/2}$ ground state multiplet, all the bands occurring in the absorption spectra become slightly narrower with decreasing temperature. However, even at low temperature the splitting of the bands is not as good as it was observed for high-symmetry systems in Nd^{3+}-doped YAG. Very recently the optical behavior of Nd^{3+} ions in new cadmium and zinc tungstate matrices were reported by us [20, 21], where the effect of narrowing bands was very weak. The bands practically did not change their widths on lowering the temperature up to 4 K. On the basis of a comparison of the compounds under investigation with those reported previously we can conclude that the disordering effect observed for Nd^{3+}-doped $La_2Mo_2O_9$ is weaker, because the differences in the width of the bands at low and room temperature are more noticeable. In case of Nd^{3+}-doped $La_2Mo_2O_9$ it is very important that the substitution of La^{3+} by Nd^{3+} takes place. Both ions possess the same valency and similar ionic radii: $Nd^{3+} = 1.163$ Å (CN = 9) is slightly smaller than La^{3+} 1.216 Å (CN = 9).

Fig. 7 presents selected $^4I_{9/2} \rightarrow {}^2P_{1/2}$, $^4I_{9/2} \rightarrow {}^4F_{3/2}$ and $^4I_{9/2} \rightarrow {}^4F_{5/2}$, $^2H_{9/2}$ transitions in the absorption spectra recorded at room and low (4 K) temperature. On the basis of the number of components observed in the bands corresponding to $^4I_{9/2} \rightarrow {}^2P_{1/2}$, $^4I_{9/2} \rightarrow {}^4F_{3/2}$ transitions we determined the number of non-equivalent positions occupied by the activator ion in 10 % Nd^{3+}-doped $La_2Mo_2O_9$. Since at 4 K only the lowest Stark component of the ground state is populated, the number of components of the Kramer doublet $^4I_{9/2} \rightarrow {}^2P_{1/2}$ transition is consistent with the number of metal sites in the crystal structure. In the samples under investigation the absorption bands corresponding to the $^4I_{9/2} \rightarrow {}^2P_{1/2}$ transition of the Nd^{3+} ion both at room as well as at low temperature possess only one component. However, this band is relatively large even at 4 K. A very similar band corresponding to the $^4I_{9/2} \rightarrow {}^2P_{1/2}$ transition, also shifted at low temperature to longer wavelengths, was reported for Nd^{3+}-doped monoclinic double molybdates [32]. The shift of the band from 430.8 nm (23 212.6 cm^{-1}) at room temperature to 431.6 nm (23 169.6 cm^{-1}) at 4 K is due to vibronic effects. Two peaks in the $^4I_{9/2} \rightarrow {}^4F_{3/2}$ doublet should be observed at 4 K. The low-temperature absorption spectra of 10 % Nd^{3+}-doped $La_2Mo_2O_9$ reveals three well resolved lines at 865.7 nm (11 551 cm^{-1}), 870.9 nm (11 482 cm^{-1}) and 877.8 nm (11 392 cm^{-1}) which correspond to $^4I_{9/2}(Z_1) \rightarrow {}^4F_{3/2}(R_2)$, $^4I_{9/2}(Z_2) \rightarrow {}^4F_{3/2}(R_2)$ and $^4I_{9/2}(Z_{1,2}) \rightarrow {}^4F_{3/2}(R_1)$ transitions, respectively. However, it can be noted that some peaks for $^4I_{9/2}(Z_1) \rightarrow {}^4F_{3/2}(R_1)$ and $(Z_1) \rightarrow {}^4F_{3/2}(R_1)$ are not resolved. Based on these results one can suggest the presence of a second perturbed site of the Nd^{3+} ion in this structure. To separate Stark components in $^4F_{3/2}(R_1)$ and $^4F_{3/2}(R_2)$ of each Nd^{3+} site it is necessary to use site-selective laser excitation and to monitor the emission intensity, as it was performed for Nd^{3+}, Nb^{5+}:$CaMoO_4$ by Andrade *et al.* [33, 34].

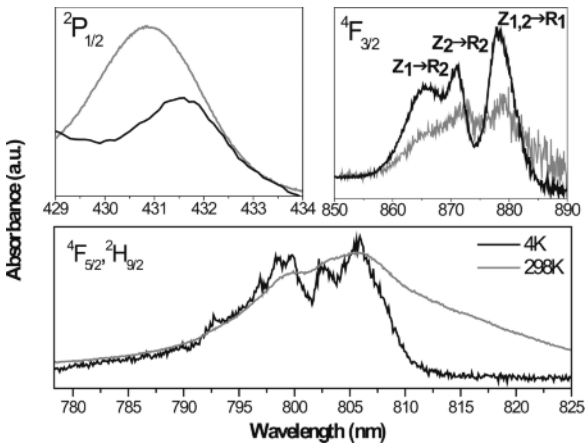

Fig. 7. Selected transitions with the determined number of non-equivalent positions occupied by the activator ion in the 10 mol-% Nd^{3+}-doped $La_2Mo_2O_9$ sample.

IR emission properties of Nd^{3+} in the $La_2Mo_2O_9$ host structure

Emission spectra also give valuable information about the structure of the compound. Samples with different concentrations of the Nd^{3+} ion (0.2 – 10 mol-%) were used. By site-selective spectroscopy the high resolution emission spectra were recorded at room temperature and 77 K using different excitation sources such as a xenon lamp (λ_{ex} = 590 nm), a tunable Ti:sapphire laser and a laser diode (λ_{ex} = 808 nm). All samples were measured under the same conditions to compare the luminescence intensity. As an example, Fig. 8 shows the emission spectra of the microcrystalline powders of 3 % Nd^{3+}-doped $La_2Mo_2O_9$ by exciting the $^4G_{5/2}$, $^2G_{7/2}$ multiplet with a Xe lamp at λ_{ex} = 590 nm. The effective phonon energy of this compound is around 868 – 952 cm^{-1} (see Fig. 4) indicating radiative relaxation of the $^4F_{3/2}$ level. The samples show a strong emission from the $^4F_{3/2}$ level to the three terms $^4I_{9/2}$ (850 – 940 nm), $^4I_{11/2}$ (1055 – 1120 nm) and $^4I_{13/2}$ (1320 – 1420 nm) of the ^4I_J multiplet with maxima at 918 nm (10 893 cm^{-1}), 1064.86 nm (9390 cm^{-1}) and 1341.81 nm (7453 cm^{-1}). The fourth transition $^4F_{3/2} \rightarrow {}^4I_{15/2}$, could not be recorded due to the limited spectral range of the spectrofluorometer.

For all samples the most intense transition is $^4F_{3/2} \rightarrow {}^4I_{11/2}$ which shows five peaks. The most intense peak is located at high energy and intensities of the other lines decrease, gradually shifting to longer wavelengths. The intensity of emission from the Nd^{3+} ion in this molybdate matrix is higher at 77 K than at room temperature.

At liquid helium temperature the emission bands, similar to the absorption bands, should be narrower. Here, the widths of the bands at room and low temperature remained the same. A very slight narrowing of the bands was observed in the absorption spectra presented

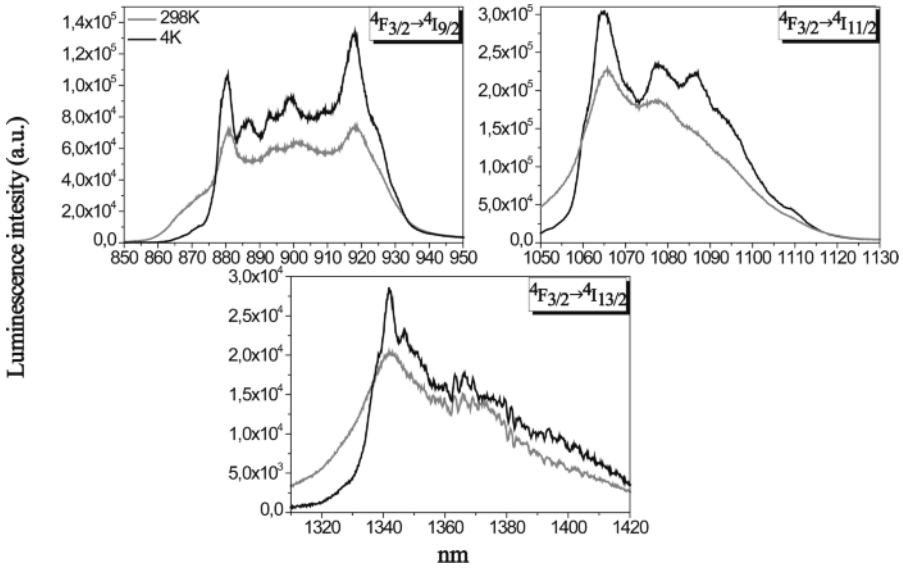

Fig. 8. Emission spectra of 3 mol-% Nd^{3+}-doped $La_2Mo_2O_9$ recorded at 77 K under Xe lamp excitation at $\lambda_{ex} = 590$ nm.

in the previous paragraph indicating a disorder of the active ions in the host. However, if we compare with the tungstates recently reported by us [20, 21], which possess also disorder in the structure, for the compounds under investigation the splitting of the bands at low temperature is better resolved.

Fig. 9 reveals the emission spectra of $La_2Mo_2O_9$ doped with different concentrations of Nd^{3+} ions (0.5 – 5 %) recorded at 77 K under a Xe lamp excitation at $\lambda_{ex} = 590$ nm. From group theoretical considerations, the $^4F_{3/2}$ multiplet splits into two Kramer's doublets, and the number of components correlates with $J + 1/2$ levels for one site. As can be seen in Figs. 8 and 9, in the spectra recorded at room and liquid nitrogen temperature, in the band corresponding to the $^4F_{3/2} \rightarrow {}^4I_{9/2}$ transition ($\lambda \approx 900$ nm) one can distinguish more than five lines (the number for the completely removed degeneracy of the $^4I_{9/2}$ level). Therefore, the number of Stark components is higher than that expected for the compound with only one symmetry site.

In the high-resolution emission spectra recorded at 77 K eight components can be observed for the $^4F_{3/2} \rightarrow {}^4I_{9/2}$ transition, and the presence of additional weak peaks indicates Nd^{3+} ions occupying another position in the structure. Both from Fig. 9 presenting low-temperature emission spectra with different concentration of optically active ions, as well as from Fig. 10, where room temperature emission spectra are presented, we can conclude that among all compounds under investigation the highest emission intensity is shown by the material containing 3 % Nd^{3+} ions. To compare the luminescence intensity of all samples, the spectra were recorded under the same conditions. The bands of highest intensity correspond to the transition $^4F_{3/2} \rightarrow {}^4I_{11/2}$ with a maximum at 1065.7 nm. The insert in Fig. 10 presents the luminescence intensity dependence on the content of the Nd^{3+} ions in $La_2Mo_2O_9$ matrix. The luminescence intensity increases up to the concentration of 3 % Nd^{3+}

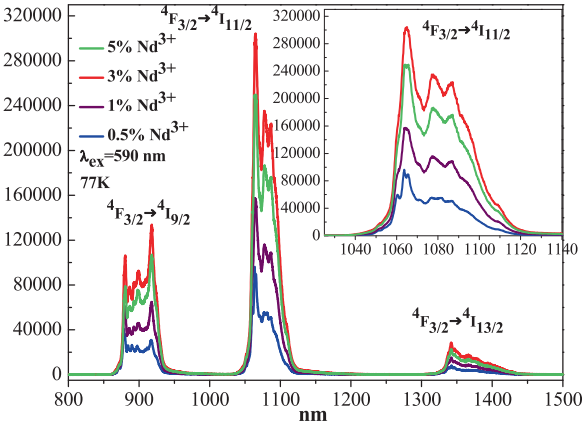

Fig. 9 (color online). Emission spectra of $La_2Mo_2O_9$ doped with different concentrations of Nd^{3+} ions (0.5 – 5 mol-%) recorded at 77 K under Xe lamp excitation at $\lambda_{ex} = 590$ nm.

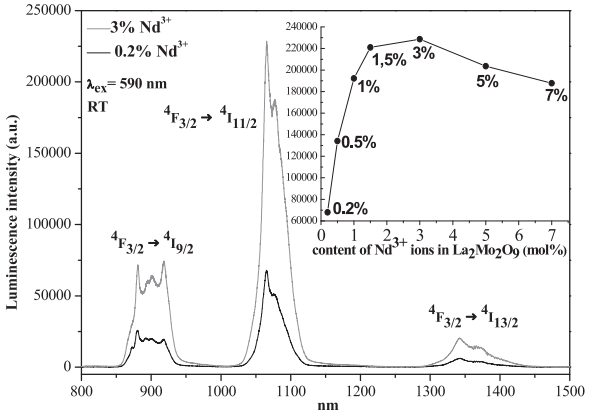

Fig. 10. Emission spectra of 0.2 and 3 mol-% Nd^{3+}-doped $La_2Mo_2O_9$ recorded at room temperature under Xe lamp excitation at $\lambda_{ex} = 590$ nm and luminescence intensity dependence of the content of Nd^{3+} ions.

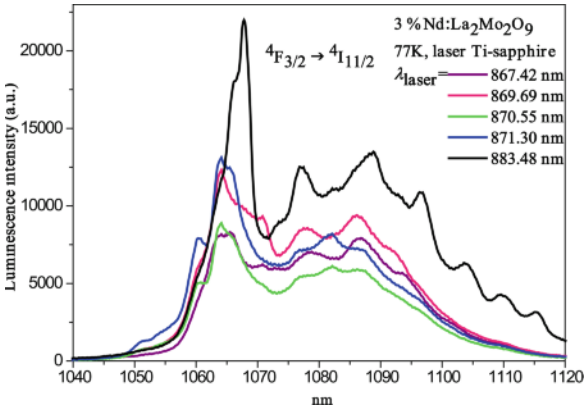

Fig. 11 (color online). Emission spectra of 3 mol-% Nd^{3+}-doped $La_2Mo_2O_9$ recorded at 77 K under Ti-sapphire laser excitation.

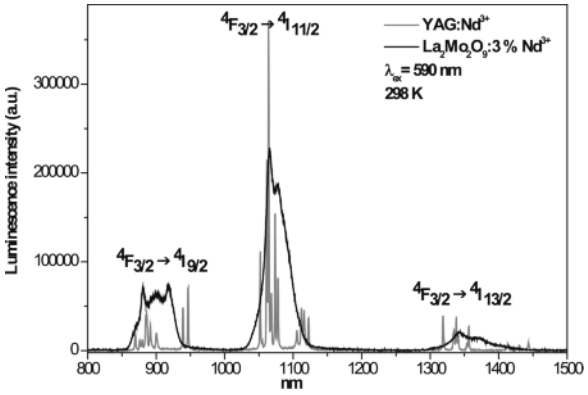

Fig. 12. Comparison of the emission spectra of 0.8 mol-% Nd^{3+}-doped $Y_3Al_5O_{12}$ (YAG:Nd^{3+}) and 3 mol-% Nd^{3+}-doped $La_2Mo_2O_9$ recorded at room temperature under Xe lamp excitation at $\lambda_{ex} = 590$ nm.

and then sequentially decreases due to the concentration quenching process by radiative and nonradiative up and down conversions well known for Nd^{3+}-doped materials.

The low-temperature emission spectra presented above, as well as the low-temperature absorption spectra (presented in the previous paragraph), allow to conclude on multisites in Nd^{3+}-doped $La_2Mo_2O_9$ solid solutions. Confirmation of this supposition one can find in low-temperature site-selective excitation spectra under laser diode and Ti-sapphire laser pumping sources. To record those spectra, extensive tuning of excitation was used. As an example, the emission spectra of 3 % Nd^{3+}-doped $La_2Mo_2O_9$ recorded at 77 K under different excitation lines of the Ti-sapphire laser is presented in Fig. 11. A comparison of the splitting and the position of the bands corresponding to the $^4F_{3/2} \rightarrow {}^4I_{11/2}$ transitions reveals the differences. One can distinguish at least three different emission spectra. This effect can also be seen for different excitations by a laser diode around $\lambda_{ex} = 808$ nm (not presented here).

Fig. 12 shows the comparison of the emission spectra of 0.8 % Nd^{3+}-doped $Y_3Al_5O_{12}$ (YAG:Nd^{3+}) and 3 % Nd^{3+}-doped $La_2Mo_2O_9$ recorded at room temperature under Xe lamp excitation at $\lambda_{ex} = 590$ nm. The emission bands in the spectral region 800 – 1500 nm for YAG:Nd^{3+} are sharper and better resolved, while for Nd^{3+}-doped $La_2Mo_2O_9$ they are very broad. The comparison of the integral intensities of the transitions for both types of compounds shows values five times (for $^4F_{3/2} \rightarrow {}^4I_{19/2}$ transition) and four times (for $^4F_{3/2} \rightarrow {}^4I_{11/2}$ transition) higher for the molybdates than for YAG:Nd^{3+}. This result indicates that the large emission spectral widths of Nd^{3+}-doped $La_2Mo_2O_9$ could be especially promising for an ultra-short pulse laser generation.

Decay times of Nd^{3+} ions in $La_2Mo_2O_9$

Fig. 13 presents the room temperature luminescence decay profiles of monoclinic Nd^{3+}-doped $La_2Mo_2O_9$ with different concentrations of Nd^{3+}. The decay curves were obtained by monitoring at 1064 nm under pulsed laser excitation at 12 376 cm^{-1} (808 nm) in the $^4F_{5/2} + {}^2H_{9/2}$ absorption levels. For the lowest

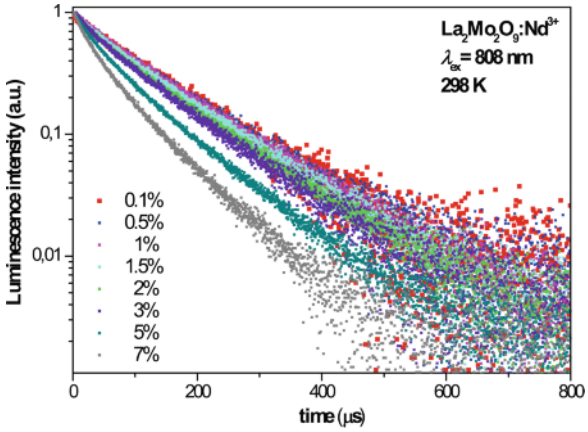

Fig. 13 (color online). Decay curves of the fluorescence from $^4F_{3/2}$ at $\lambda_{em} = 1064$ nm of monoclinic Nd^{3+}-doped (0.1, 0.5, 1, 1.5, 2, 3, 5 and 7 mol-%) $La_2Mo_2O_9$ measured at room temperature at $\lambda_{ex} = 808$ nm.

concentration (0.1 %) the decay curves which are exponential with a fitted lifetime of about 120 μs both at room and low temperature, correspond to the radiative lifetime.

When the concentration increases, the decays are strongly non-exponential, and we have measured the integrated lifetimes. At room temperature, about 75 μs were determined for the 5 % Nd^{3+}, and about 46 μs for the 7 % Nd^{3+} sample, indicating a concentration quenching process. The decay curves were recorded also at low temperature where the values of the integrated lifetimes are slightly higher. The decay curves for the samples with higher concentrations (5, 7 and 10 %) of Nd^{3+} ion become also non-exponential. The non-exponential character is enhanced at the highest concentration pointing at a fluorescence quenching owing to the well-known energy transfer between the Nd^{3+} ions by the usual up/down conversion and cross-relaxation mechanisms for greater numbers of Nd^{3+} levels.

Conclusions

A series of Nd^{3+}-doped $La_2Mo_2O_9$ samples with different concentrations of the optically active ion was obtained *via* high-temperature solid-state reactions. The analysis using both powder X-ray diffraction and FT-IR spectroscopy has confirmed the formation of a $La_2Mo_2O_9$ phase which crystallizes in the low-temperature monoclinic α-form when the concentration of Nd^{3+} is up to 10 mol-%. The SEM images show high homogeneity of irregularly shaped products, with a grain size in the range of 3 – 8 μm. In the absorption spectra the highest intensity is observed for the hypersensitive $^4I_{9/2} \rightarrow {}^4G_{5/2}, {}^2G_{7/2}$ transitions. The intensity ratio between two bands in the IR spectral ranges 710 – 778 nm and 778 – 838 nm, and the one at 550 – 617 nm of about 1 : 2, which is very similar both at room and low temperature, indicates high symmetry for the system under investigation. The $^4I_{9/2} \rightarrow {}^2P_{1/2}$ transition at low temperature (4 K) consists of only one component which suggests only one symmetry site of Nd^{3+} in this compound. However this band is relatively broad and asymmetric. As a consequence, it is difficult to assess the exact number of components, as they may overlap quite substantially. Very important information comes from the number of components observed for the $^4I_{9/2} \rightarrow {}^4F_{3/2}$ doublet in the absorption spectra. The three well resolved lines at 865.7, 870.9 and 877.8 nm point to the presence of at least two non-equivalent perturbed Nd^{3+} sites. The multisite character was also confirmed by the high resolution site-selective emission spectra. By using different excitation lines one can distinguish between at least three sets each presenting differently shaped emissions. The number of Stark components in the emission spectra is higher than that expected for a compound with only one symmetry site. The Nd^{3+}-doped $La_2Mo_2O_9$ molybdates exhibit structural disorder resulting in a significant inhomogeneous broadening of the spectral bands visible in the absorption and emission spectra. Due to both down- and upconversion transfers, the concentration dependence of the emission intensities and fluorescence lifetimes (from 120 μs for the low-concentrated samples to tens of μs for more concentrated ones) confirm a strong concentration quenching of the Nd^{3+} emission. The values of integrated emission intensities measured for Nd^{3+}-doped molybdates are higher than those determined for Nd^{3+}-doped YAG. The structural disorder that causes broadening of absorption and emission lines can be useful for pumping of Nd^{3+} ions with laser diode sources which have the drawback of a thermal shift of the laser emission. The broad spectral emission band in the investigated molybdates might allow both the tuning of laser radiation over the 1030 – 1080 nm range and the generation of ultra-short pulses, which could find applications in pico- or even femtosecond lasers.

Acknowledgement

We wish to thank the Minister of Science and Higher Education in Poland and in France for the Grant POLONIUM for scientific exchange between Institute Light Matter (ILM), UMR5306 CNRS-University Lyon1, University of Lyon, France, and Faculty of Chemistry, University of Wrocław in Poland. This financial support is gratefully acknowledged.

[1] A. A. Kaminski, *Crystalline Lasers: Physical Processes and Operating Schemes*, CRC Press, Boca Raton **1996**.
[2] A. A. Kaminski, A. A. Pavlyuk, T. I. Butaeva, L. I. Bobovich, V. V. Lyubchenco, *Neorg. Mater.* **1979**, *15*, 541.
[3] M. C. Pujol, R. Sole, J. Massons, J. Gavalda, X. Solans, F. Dias, M. Aguilo, *J. Appl. Crystallogr.* **2002**, *35*, 108.
[4] G. Boulon, G. Metrat, N. Muhlstein, A. Brenier, M. R. Kokta, L. Kravchik, Y. Kalisky, *Opt. Mater.* **2003**, *24*, 377.
[5] A. Brenier, F. Bourgeois, G. Metrat, N. Muhlstein, G. Boulon, *Opt. Mater.* **2001**, *16*, 207.
[6] G. Metrat, N. Muhlstein, A. Brenier, G. Boulon, *Opt. Mater.* **1997**, *8*, 75.
[7] R. Kawai, Y. Miyasaka, K. Otsuka, T. Ohtomo, T. Narita, J.-Y. Ko, I. Shoji, T. Taira, *Opt. Express* **2004**, *12*, 2293.
[8] A. Ikesue, I. Furusato, K. Kamata, *J. Am. Ceram. Soc.* **1995**, *78*, 225.
[9] A. Ikesue, T. Kinoshita, K. Kamata, K. Yoshida, *J. Am. Ceram. Soc.* **1995**, *78*, 1033.
[10] J. R. Lu, K. Ueda, H. Yagi, T. Yanagitani, T. Akiyama, A. A. Kaminskii, *J. Alloys Compd.* **2002**, *341*, 220.
[11] Y. Rabinovitch, D. Tetard, M. D. Faucher, M. Pham-Thi, *Opt. Mater.* **2003**, *24*, 345.
[12] M. Dubinskiy, L. D. Merkle, J. R. Goff, G. J. Quarles, V. K. Castillo, K. L. Schepler, D. Zelmon, S. Guha, L. P. Gonzalez, M. R. Rickey, J. J. Lee, S. M. Hegde, J. Q. Dumm, G. L. Messing, S.-H. Lee, *Proc. SPIE* **2005**, *5792*, 1.
[13] S. Georges, F. Goutenoire, F. Altorfer, D. Sheptyakov, F. Fauth, E. Suard, P. Lacorre, *Solid State Ionics* **2003**, *161*, 231.
[14] J. P. Fournier, J. Fournier, R. Kohlmuller, *Bull. Soc. Chim. Fr.* **1970**, *12*, 4277.
[15] P. Lacorre, R. Retoux, *J. Solid State Chem.* **1997**, *132*, 443.
[16] W. Kuang, Y. Fan, K. Yao, Y. Chen, *J. Solid State Chem.* **1998**, *140*, 354.
[17] F. Goutenoire, O. Isnard, R. Retoux, P. Lacorre, *Chem. Mater.* **2000**, *12*, 2575.
[18] G. Corbel, P. Durand, P. Lacorre, *J. Solid State Chem.* **2009**, *182*, 1009.
[19] G. Corbel, E. Chevereau, S. Kodjikian, P. Lacorre, *Inorg. Chem.* **2007**, 46, 6395.
[20] M. Guzik, J. Cybińska, E. Tomaszewicz, Y. Guyot, J. Legendziewicz, G. Boulon, W. Stręk, *Opt. Mater.* **2011**, *34*, 487.
[21] M. Guzik, E. Tomaszewicz, Y. Guyot, J. Legendziewicz, G. Boulon, *J. Mater. Chem.* **2012**, *22*, 14896.
[22] I. Radosavljevic Evans, J. A. K. Howard, J. S. O. Evans, *Chem. Mater.* **2005**, *17*, 4074.
[23] F. Goutenoire, O. Isnard, E. Suard, O. Bohnke, Y. Laligant, R. Retoux, P. Laccore, *J. Mater. Chem.* **2011**, *11*, 119.
[24] A. Arulraj, F. Goutenoire, M. Tabellout, O. Bohnke, P. Lacorre, *Chem. Mater.* **2002**, *14*, 2492.
[25] V. I. Tsaryuk, V. F. Zolin, *Spectrochim. Acta A* **2001**, *57*, 355.
[26] N. Mhadhbi, Doctoral Thesis, University of Maine, Maine, France, **2012**.
[27] L. Seguin, M. Figarz, R. Cavaganat, J. C. Lassègues, *Spectrochim. Acta A* **1995**, *51*, 1323.
[28] T. T. Basiev, A. Sobol, Y. K. Voronko, P. G. Zverev, *Opt. Mater.* **2000**, *15*, 205.
[29] G. D. Saraiva, W. Paraguassu, M. Maczka, P. T. C. Freire, J. A. Lima, C. W. A. Paschoal, J. Filho, A. Filho, *J. Raman Spectrosc.* **2008**, *39*, 937.
[30] E. Galdecka, Z. Galdecki, E. Huskowska, V. Amirkhanov, J. Legendziewicz, *J. Alloys Compd.* **1997**, *257*, 182.
[31] J. Legendziewicz, *Acta Phys. Pol., A* **1996**, *90*, 127.
[32] L. Macalik, J. Hanuza, J. Legendziewicz, *Acta Phys. Pol., A* **1993**, *84*, 909.
[33] L. H. C. Andrade, M. Siu Li, Y. Guyot, A. Brenier, G. Boulon, *J. Phys.: Condens. Matter* **2006**, *18*, 7883.
[34] L. H. C. Andrade, D. Reyes Ardila, L. B. Barbosa, J. P. Andreeta, M. Siu Li, A. Brenier, Y. Guyot, G. Boulon, *Eur. Phys. J.: Appl. Phys.* **2005**, *29*, 55.